

Apoptotic Vesicles Regulate Bone Metabolism via the miR1324/SNX14/SMAD1/5 Signaling Axis

Yuan Zhu, Kunkun Yang, Yawen Cheng, Yaoshan Liu, Ranli Gu, Xuenan Liu, Hao Liu, Xiao Zhang,* and Yunsong Liu*

Mesenchymal stem cells (MSCs) are widely used in the treatment of diseases. After their *in vivo* application, MSCs undergo apoptosis and release apoptotic vesicles (apoVs). This study investigates the role of apoVs derived from human bone marrow mesenchymal stem cells (hBMMSCs) in bone metabolism and the molecular mechanism of the observed effects. The results show that apoVs can promote osteogenesis and inhibit osteoclast formation *in vitro* and *in vivo*. ApoVs may therefore attenuate the bone loss caused by primary and secondary osteoporosis and stimulate bone regeneration in areas of bone defect. The mechanisms responsible for apoV-induced bone regeneration include the release of miR1324, which inhibit expression of the target gene Sorting Nexin 14 (SNX14) and thus activate the SMAD1/5 pathway in target cells. Given that MSC-derived apoVs are easily obtained and stored, with low risks of immunological rejection and neoplastic transformation, The findings suggest a novel therapeutic strategy to treat bone loss, including via cell-free approaches to bone tissue engineering.

Mesenchymal stem cells (MSCs) are easily isolated from tissues and have the ability to self-proliferate and to differentiate along different cell lineages, such that they are commonly used in tissue regeneration.^[10–14] Several clinical studies have shown that MSCs are safe and effective when used in tissue repair and wound healing.^[15–21] However, despite the therapeutic efficacy of MSCs, there are significant costs and challenges associated with their therapeutic use, because they require strict monitoring of manufacturing, processing, and storage to ensure optimal viability and potency following transplantation.^[22,23] Some studies have shown that stem cells transplanted into the body initially undergo significant apoptosis^[24–29] and that the direct transplantation of apoptotic stem cells can have lasting effects.^[30]

Apoptosis plays an important role in maintaining physiological homeostasis.^[31–33] Apoptotic vesicles (apoVs) are extracellular vesicles rich in proteins, RNA, and lipids that are released during apoptosis.^[34] Their role is to mediate the transfer of substances and signal exchange between cells and thus maintain homeostasis. In a previous study, we examined the characteristics and specific markers of MSC-derived apoVs and found that proteins on the surface of apoVs regulated platelet aggregation.^[35] In another study, we demonstrated the therapeutic effect of MSC-derived apoVs, including in type 2 diabetes, through their interactions with hepatic macrophages.^[36] We also found that apoVs activate the Fas pathway in multiple myeloma cells and thus induce apoptosis in these tumor cells.^[37] Pluripotent stem cell (PSC)-derived apoVs (PSC-apoVs) can inherit pluripotent molecules from PSCs to stimulate adult stem cells and promote wound healing in mouse skin.^[38] Exogenous apoVs (apoEVs) have been reported to promote wound healing and hair growth by activating the Wnt/ β -catenin pathway.^[39] The administration of apoVs can prevent Th17 differentiation and memory T cell formation to ameliorate inflammation and joint erosion in a mouse model of arthritis.^[40] While mouse MSC-derived apoVs has been used to treat osteoporosis,^[41] whether apoVs derived from human bone marrow mesenchymal stem cells (hBMMSCs) can impact bone metabolism is unknown. Thus, we investigated the regulatory role of apoVs in bone metabolism and therapeutic effects on bone defects and bone loss. Our results provide an important theoretical basis for novel clinical applications of hBMMSCs-derived apoVs.

1. Introduction

Bone homeostasis is maintained by the balance between bone formation and bone resorption.^[1–5] Some clinical conditions, such as bone fractures, osteoporosis, and tumor resection, can lead to bone defects or bone loss. If the critical defect size is exceeded, the ability of bone to repair and regenerate itself is limited.^[6–9]

Y. Zhu, K. Yang, Y. Cheng, Y. Liu, R. Gu, X. Liu, X. Zhang, Y. Liu
Department of Prosthodontics
Peking University School and Hospital of Stomatology
22 Zhongguancun South Avenue, Beijing 100081, China
E-mail: kqxiaozhang@hsc.pku.edu.cn; liuyunsong@hsc.pku.edu.cn

H. Liu
The Central Laboratory
Peking University School and Hospital of Stomatology
22 Zhongguancun South Avenue, Beijing 100081, China
Y. Zhu, X. Zhang, Y. Liu
National Center of Stomatology
National Laboratory for Digital and Material Technology of Stomatology
National Clinical Research Center for Oral Diseases
Beijing Key Laboratory of Digital Stomatology
Peking University School and Hospital of Stomatology
Beijing 100081, China

 The ORCID identification number(s) for the author(s) of this article can be found under <https://doi.org/10.1002/smll.202205813>.

DOI: 10.1002/smll.202205813

2. Results and Discussion

2.1. Characterization of hBMMSC-Derived apoVs

Following the method employed in previous study,^[35] apoptosis in hBMMSCs was induced using staurosporine (STS) and the apoptotic hBMMSCs were compared to control non-apoptotic hBMMSCs by fluorescence microscopy and TUNEL staining, as a measure of apoptosis^[42] (Figure 1). A much larger number of TUNEL-positive cells was observed in the STS group than in the control group. Transmission electron microscopy (TEM) showed the cup-shaped morphology of the apoVs. The nanoparticle tracking analysis (NTA) showed that the diameter distribution range of apoVs was 199.3 ± 91.3 nm. Flow cytometry showed the presence of Annexin V on the membrane surface of the apoVs, together with the extracellular vesicle markers CD9, CD63, and CD81, and the MSC markers CD29(+), CD44(+), CD90(+), CD34(-), and CD45(-). In Western blotting analysis, a high-level expression of EV markers (CD9, CD63, and CD81) was detected. Moreover, the specific protein markers for MSC-derived apoVs, like Fas, Integrin alpha-5, CD44, and Calreticulin, were enriched in hBMMSC-apoVs, which was consistent with our previous study.^[35]

2.2. hBMMSC-Derived apoV Uptake by MSCs

The uptake of hBMMSC-derived apoVs by MSCs was investigated by incubating the cells with PKH-26-labeled apoVs for 2 to 72 h. MSC nuclei were stained with DAPI, and cellular F-actin with phalloidin. Confocal laser scanning microscopy (CLSM) indicated a gradual increase in apoVs around the MSCs nucleus between 2 and 24 h, with a decrease thereafter, perhaps as a result of the host cells' metabolism (Figure 2). In previous work, we found that exosomes are taken up by MSCs, where they have regulatory effects.^[43,44] Similarly, the present results demonstrate that apoVs are taken up by MSCs.

2.3. hBMMSC-Derived apoVs Promote MSC Osteogenesis

A CCK8 assay showed that apoVs at concentrations of $0-0.8 \mu\text{g mL}^{-1}$ were not significantly toxic to MSCs (Figure S1A, Supporting Information). To investigate how hBMMSC-derived apoVs affected osteogenesis, MSCs were cultured in osteogenic medium (OM) and then given the apoV treatment. ALP and ARS staining showed that $0.2 \mu\text{g apoVs mL}^{-1}$ had a pronounced osteogenic effect on MSCs; this concentration was therefore used in subsequent experiments (Figure S1B, Supporting Information). Because cell migration was a crucial step in wound healing, a scratch wound assay was used to investigate the effect of apoVs on MSC migration. Migration was enhanced by adding apoVs to the culture medium (Figure S2, Supporting Information). ApoVs had no discernible impact on MSC proliferation in a CCK8 assay. Alkaline Phosphatase (ALP) staining and quantification showed that apoVs greatly improved the osteogenic differentiation of MSCs after 7 days of incubation in OM (Figure 3). The same results were obtained with Alizarin Red S (ARS) staining and quantification on day 14. ALP,

RUNX2, and BGLAP are markers used to monitor stem cell osteogenesis.^[45] In MSCs treated with apoVs, the expression of ALP and RUNX2 increased significantly after 7 days and that of RUNX2 and BGLAP after 14 days. Western blotting showed that RUNX2 expression was upregulated in apoV-treated cells during osteogenesis. To determine the role of hBMMSC-derived apoVs in MSC osteogenesis *in vivo*, MSCs cultured with or without apoVs were mixed with β -tricalcium phosphate (β -TCP) and implanted into nude mice. Hematoxylin-eosin (H&E) and Masson staining indicated more bone tissue-like structures and more collagen fibers in the apoV-treated group than the control group. Together, the results demonstrate the ability of hBMMSC-derived apoVs to promote MSC osteogenesis *in vitro* and *in vivo*. The differentiation of stem cells is influenced by both internal and external factors.^[46-48] Methods to promote the stem cell osteogenesis to efficiently build tissue-engineered bone have become a topic of intense research.^[49,50] Our study demonstrates the potential of apoVs in bone tissue engineering.

2.4. hBMMSC-Derived apoVs Attenuate Bone Loss Induced by Estrogen Deficiency in OVX mice

Osteoporosis (OP) is a bone disease in which the reduced bone mass and the destruction of the bone microarchitecture increase bone fragility and the susceptibility to fracture. The disease is caused by an imbalance in the processes of osteoblast-mediated bone formation and osteoclast-mediated bone resorption.^[51-54] Therefore, we explored the effect of hBMMSC-derived apoVs on bone loss in ovariectomized (OVX) mice, a commonly used animal model of OP. First, we set different concentration gradients, and the results showed that there was a significant increase in bone mass after apoV injection. We found that the injection of $20 \mu\text{g apoVs per } 30 \text{ g weight}$ showed the highest efficiency in bone repair, so we used this concentration for subsequent *in vivo* experiments (Figure S3, Supporting Information). Knowledge of the biodistribution of apoVs is particularly important in the design of EVs for therapeutic purposes to determine the targeting level of apoVs as well as off-target effects.^[55] We injected DiR-apoVs into mice via the tail vein and monitored the distribution of fluorescent signals in the major organs of the mice. At 24, 48, and 72 h post-injection, whole-body fluorescence imaging (Figure S4, Supporting Information) showed that the apoVs were mostly enriched in the liver, which implies their hepatic metabolism after injection, consistent with previous findings.^[39] Over time, apoV enrichment in the femur gradually increased. While some studies have reported that EVs from different cellular sources that differ in their biodistribution patterns,^[56,57] EVs usually accumulate in the liver, lungs, kidneys, and spleen. Therefore, the therapeutic use of apoVs in other organs and tissues will require their modification to increase their specific recognition and thus their therapeutic effect.

The histomorphology of the femur was evaluated via micro-CT (Figure 4). In the OVX + apoVs group, trabecular BMD (Tb. BMD), bone volume (BV)/total volume (TV), trabecular thickness (Tb.Th), and trabecular number (Tb.N) were significantly increased compared to the OVX group. In addition, bone surface area (BS/BV) and trabecular separation (Tb.Sp) were mark-

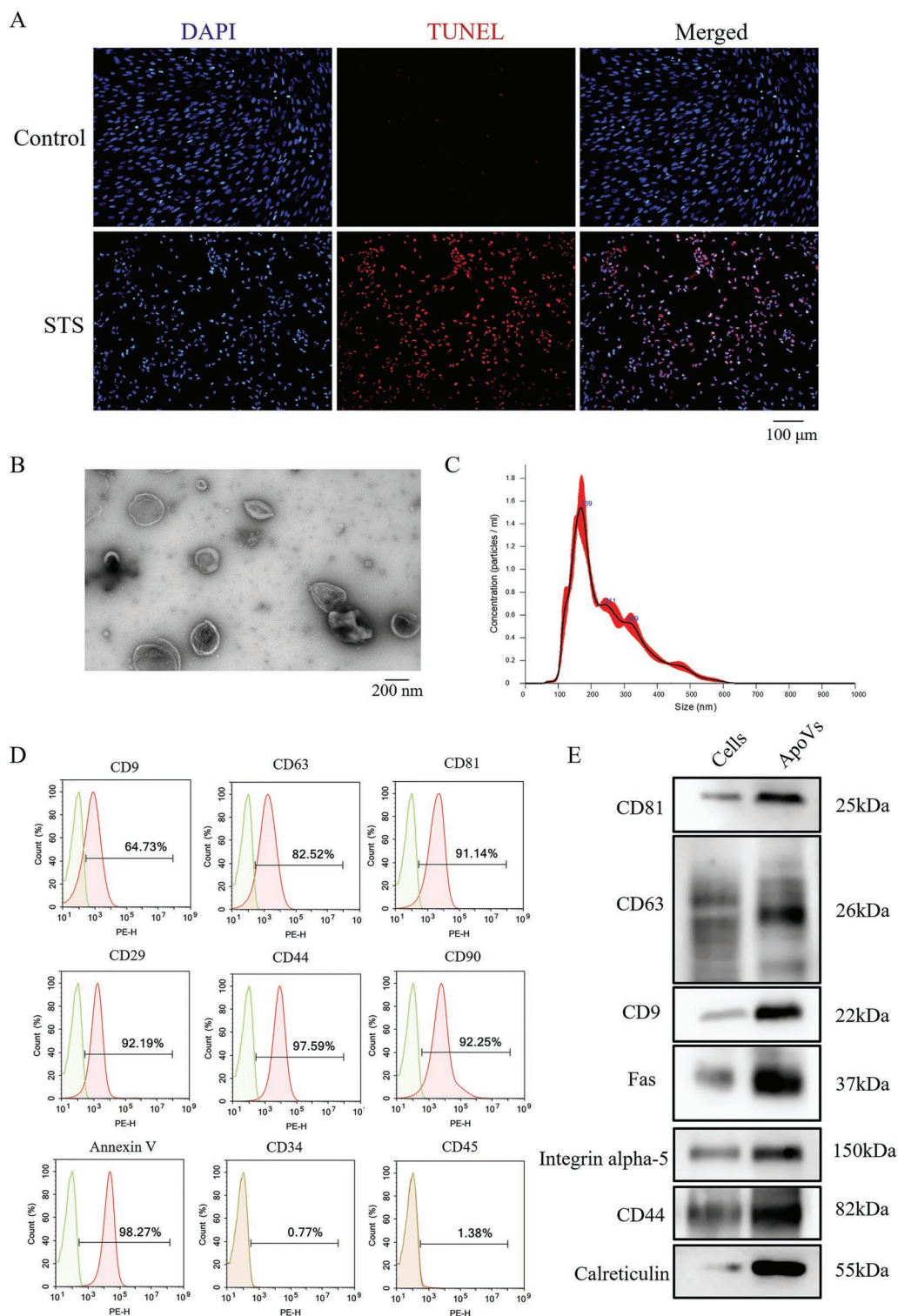


Figure 1. Characterization of hBMMSC-derived apoVs. A) TUNEL staining in sections from the different groups. B) Morphology of apoVs. C) Particle size distribution of apoVs. D) Flow cytometric analysis. E) Western blotting showed the expressions of CD9, CD63, CD81, Fas, Integrin alpha-5, CD44, and Calreticulin of hBMMSCs and apoVs.

edly lower in the OVX + apoVs group than in the OVX group. In the OVX group, there were significant decreases in femoral Tb.BMD, BV/TV, Tb.Th, and Tb.N, and significant increases

in BS/BV and Tb.Sp compared to the sham-operated group. H&E and Masson staining confirmed that apoVs attenuated the bone loss induced by estrogen deficiency in OVX mice. Double

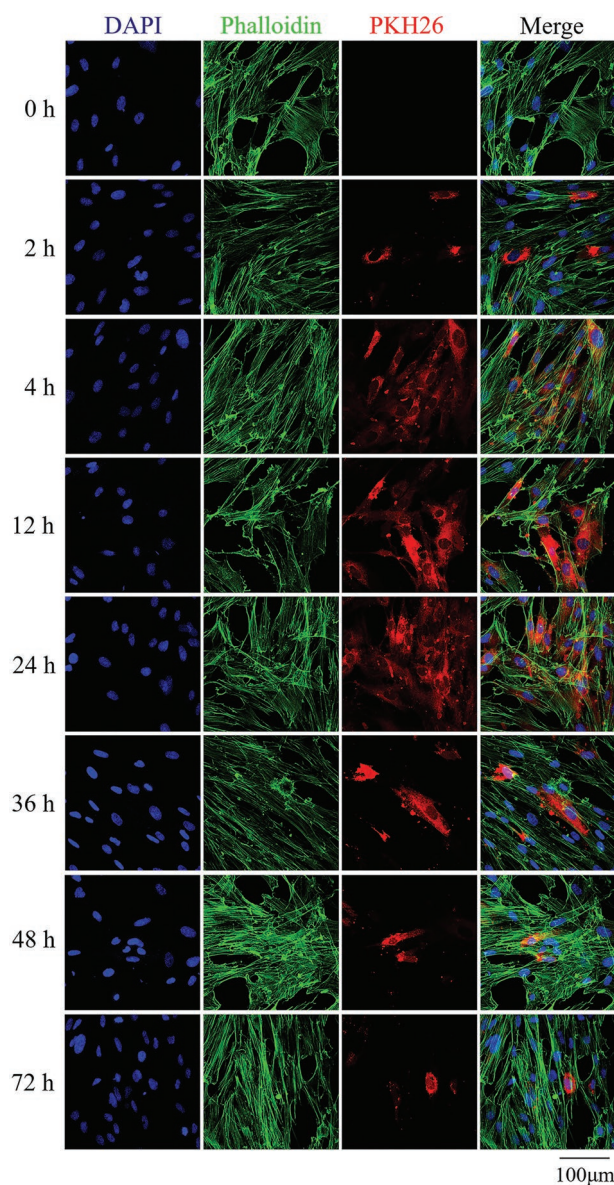


Figure 2. Uptake of PKH-26-labeled apoVs (red) by MSCs. MSC nuclei were stained with DAPI (blue), and cellular F-actin with phalloidin (green).

fluorescence labeling, used to analyze dynamic histomorphometry, showed a higher mineral apposition rate (MAR) in the OVX + apoVs group than in the OVX group. H&E staining of mouse viscera showed that apoVs were not toxic to the mice (Figure S5, Supporting Information). BMMSCs were extracted from the femurs of mice in the different groups (mBMMSCs), cultured in proliferation medium (PM) and OM, and stained with ALP and ARS. ApoVs significantly promoted mBMMSCs osteogenesis, as indicated by ALP and ARS staining. The results indicate that apoVs treatment attenuates the osteoporotic phenotype of OVX mice by rescuing the function of endogenous mBMMSCs. Besides, we found that OVX MSCs showed reduced osteogenic capacity compared to normal MSCs (Figure 4G,H), which was consistent with the previous report.^[58] The biological functions of apoVs strongly depend on

the identity of their parental cells. Therefore, it is reasonable to speculate that the effect of apoVs derived from OVX MSCs on osteogenesis is inferior to normal apoVs.

2.5. hBMMSC-Derived apoVs Prevent Bone Mass Decrease and Bone Microarchitecture Deterioration in Aged Mice

Age-related OP is characterized by a deterioration in bone mass and strength, attributed to a dysfunction of BMMSCs during aging.^[59,60] We, therefore, explored the effect of hBMMSC-derived apoVs on the aging-related decrease in bone mass and the deterioration of bone microarchitecture, using micro-CT to examine the histomorphology of the femur (Figure 5). In the aged + apoVs group, Tb.BMD, BV/TV, Tb.Th, and Tb.N were significantly higher, and BS/BV and Tb.Sp significantly lower than in the aged group. H&E and Masson staining indicated that apoVs prevented both a decrease in bone mass and the deterioration of bone microarchitecture in aged mice. Double fluorescence labeling showed a higher MAR in the aged + apoVs group than in the aged group. ALP and ARS staining of mBMMSCs extracted from the femurs of mice in the different groups and then cultured in PM and OM showed that apoVs significantly promoted osteogenic differentiation of mBMMSCs. This suggests that apoVs ameliorate the osteoporotic phenotype while promoting mBMMSC osteogenesis in aged mice.

2.6. hBMMSC-Derived apoVs Increase Bone Formation in Rat Calvarial Defects

PLGA/pDA scaffolds were incubated with PKH-26-labeled apoVs and examined by CLSM, which revealed an even distribution of immobilized apoVs on the scaffold surface, with more labeling of the PLGA/pDA than of the PLGA scaffold (Figure S6, Supporting Information). Scanning electron microscopy (SEM) showed the much larger number of apoVs and the refractive morphology of the apoVs distributed on the surface of the PLGA/pDA than the PLGA group. Each scaffold contained $30 \pm 6.5 \mu\text{g}$ apoVs, which were only slowly released from the scaffold.

Next, we used a rat model of a skull defect to study the biological role of apoVs in promoting bone formation. PLGA/pDA scaffolds with or without apoVs were implanted in rats with a skull defect. Micro-CT showed that the defect was almost completely unhealed in the blank group, while in the scaffold group, a small cluster of high-density spots was observed. By contrast, in the apoVs group, large areas of new bone had formed along the edges of the bone defect (Figure 6). Quantification of micro-CT images further demonstrated that significantly more new bone was formed in the apoVs group than in the scaffold or blank group. H&E and Masson staining confirmed the presence of more new bone tissue in the apoVs group than in the other groups. An immunofluorescence analysis showed a significantly greater amount of RUNX2-positive cells in the apoVs group than PLGA/pDA group. The apoVs did not induce any adverse reactions in the rats, nor was an inflammatory infiltrate observed in viscera slices (Figure S7, Supporting Information). To investigate

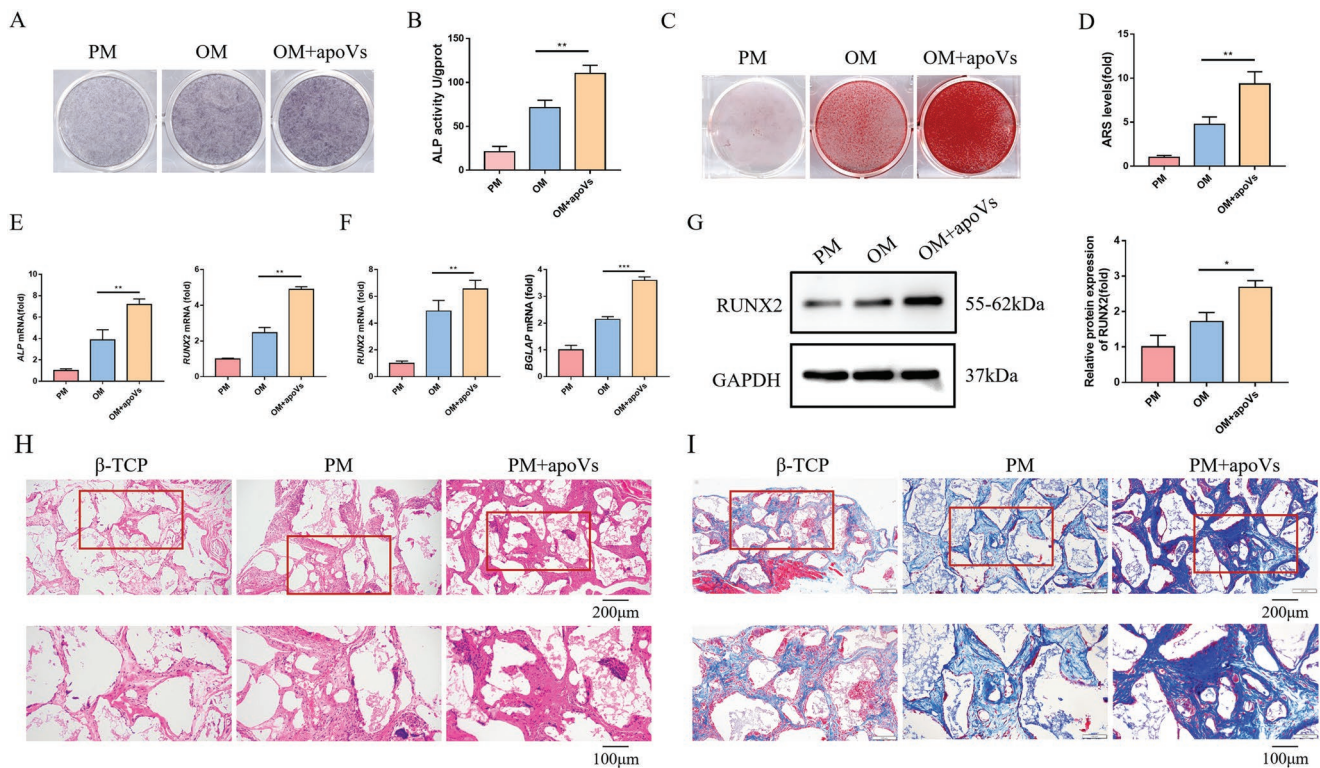


Figure 3. hBMMSC-derived apoVs promote osteogenesis in MSCs. ApoVs promote MSC osteogenesis as indicated by: A) ALP staining, B) ALP quantification, C) ARS staining, and D) ARS quantification. RT-qPCR showed that ApoVs promote the expression of: E) ALP and RUNX2 on day 7 of the incubation and F) RUNX2 and BGLAP on day 14 of the incubation. The result was confirmed by G) Western blotting. H) H&E and I) Masson staining. The red rectangles indicate the corresponding magnified areas. * $P < 0.05$, ** $P < 0.01$, *** $P < 0.001$. $N \geq 5$ per group.

the mechanism of action of the apoVs in repairing the calvarial defect, we examined the ability of the apoVs to recruit host MSCs *in vivo*. CD73 positive and CD45 negative cells were used as markers of MSCs. As shown in Figure 6E, a significantly higher proportion of MSCs was associated with the scaffold of the PLGA/pDA + apoVs group. During bone regeneration, endogenous MSCs are recruited to the site of injury, where they function as the primary healing cells.^[61,62] In a previous study, we observed that pDA/PLGA increases the adhesion of exosomes, which are then only slowly released. The locally applied exosomes are then able to promote the chemotactic homing, proliferation, and osteogenic differentiation of MSCs, thereby facilitating bone defect repair.^[45] BMSC-derived exosomes were also shown to promote the proliferation and migration of tendon stem/progenitor cells.^[63] Our results demonstrate the ability of apoVs to significantly promote the repair of *in situ* bone defects, by chemotactically recruiting MSCs. Thus, cell-free tissue-engineered bone constructed with apoVs as the core largely fulfills the conditions required of a material suitable for bone tissue engineering, including the repair of critical bone defects.

2.7. hBMMSC-Derived apoVs Inhibit Bone Resorption

The balance between bone formation by osteoblasts and bone resorption by osteoclasts is important for maintaining bone mass.^[64] Osteoblasts differentiate from MSCs and aggregate along the bone surface, where they differentiate into osteo-

cytes.^[65] Osteoclast precursor cells, derived from hematopoietic monocyte/macrophages, undergo cell fusion via key cytokines to form multinucleated cells with bone resorption capacity.^[3] Dysregulated bone remodeling leads not only to OP but also to other skeletal disorders, both genetic and acquired, and has therefore attracted considerable research into its mechanism and treatment.^[66–68] Thus, in further tests we analyzed the role of apoVs in bone regeneration *in vitro*. The uptake of hBMMSC-derived apoVs by RAW264.7 was investigated by incubating the cells with PKH-26-labeled apoVs for 2 to 72 h. RAW264.7 nuclei were stained with DAPI, and cellular F-actin with phalloidin. CLSM indicated a gradual increase in apoVs around the RAW264.7 nucleus between 2 and 36 h, with a decrease thereafter (Figure S8, Supporting Information). RAW264.7 cells cultured in osteoclastic medium (OCM) were induced to differentiate into osteoclasts by adding RANKL and then treating them with apoVs, or not. Tartrate-resistant acid phosphatase (TRAP) staining and fluorescence staining showed a significant reduction of osteoclast number in the OCM + apoVs group than in the OCM group (Figure 7A,B). In a bone resorption assay, bone resorption area was significantly smaller in the OCM + apoVs group than in the OCM group (Figure 7C). In a parallel *in vivo* analysis, femoral TRAP staining similarly showed significantly fewer TRAP-positive cells in the femur of OVX mice injected with apoVs (Figure 7D). Together, these results suggest that apoVs inhibit osteoclast formation and bone resorption *in vitro* and *in vivo*. Exosomes are closely linked with bone homeostasis and osteoblasts secrete RANKL-rich exosomes that target monocytes.^[69]

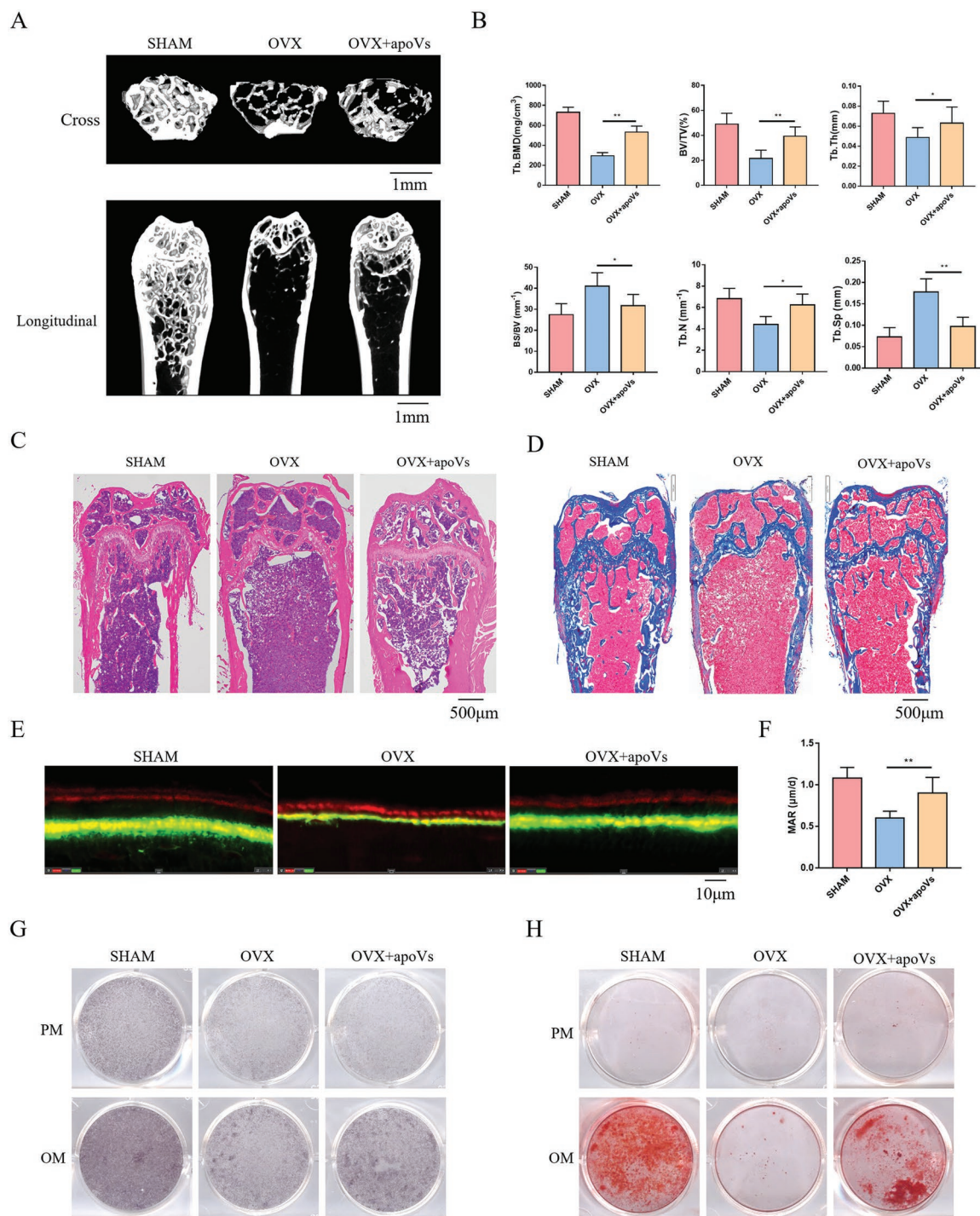


Figure 4. ApoVs attenuate bone loss induced by estrogen deficiency in OVX mice. A) Representative images of the femur reconstructed by micro-CT. B) Bone histomorphometry of the femur. C) H&E staining. D) Masson staining. E) Representative fluorescence images of the femur obtained after double labeling. F) Dynamic MAR measured from the femur. mBMMSCs extracted from mouse femurs from the different groups were stained G) with ALP on day 7 and H) with ARS on day 14. * $P < 0.05$, ** $P < 0.01$. $N \geq 5$ per group.

RANKL-RANK binding on the monocyte surface then activates osteoclastogenesis.^[70,71] Monocytes have also been shown to secrete exosomes that promote osteoclast differentiation.^[72] These results demonstrate that apoVs regulate osteoclast differentiation and, in turn, bone homeostasis.

2.8. MiR1324 Promotes Osteogenesis by MSCs

EVs contain proteins, lipids, DNA, and RNA,^[73,74] with the latter made up of mRNAs, miRNAs, and ncRNAs. Nearly half of the RNA content of EVs consists of miRNA, which is involved in

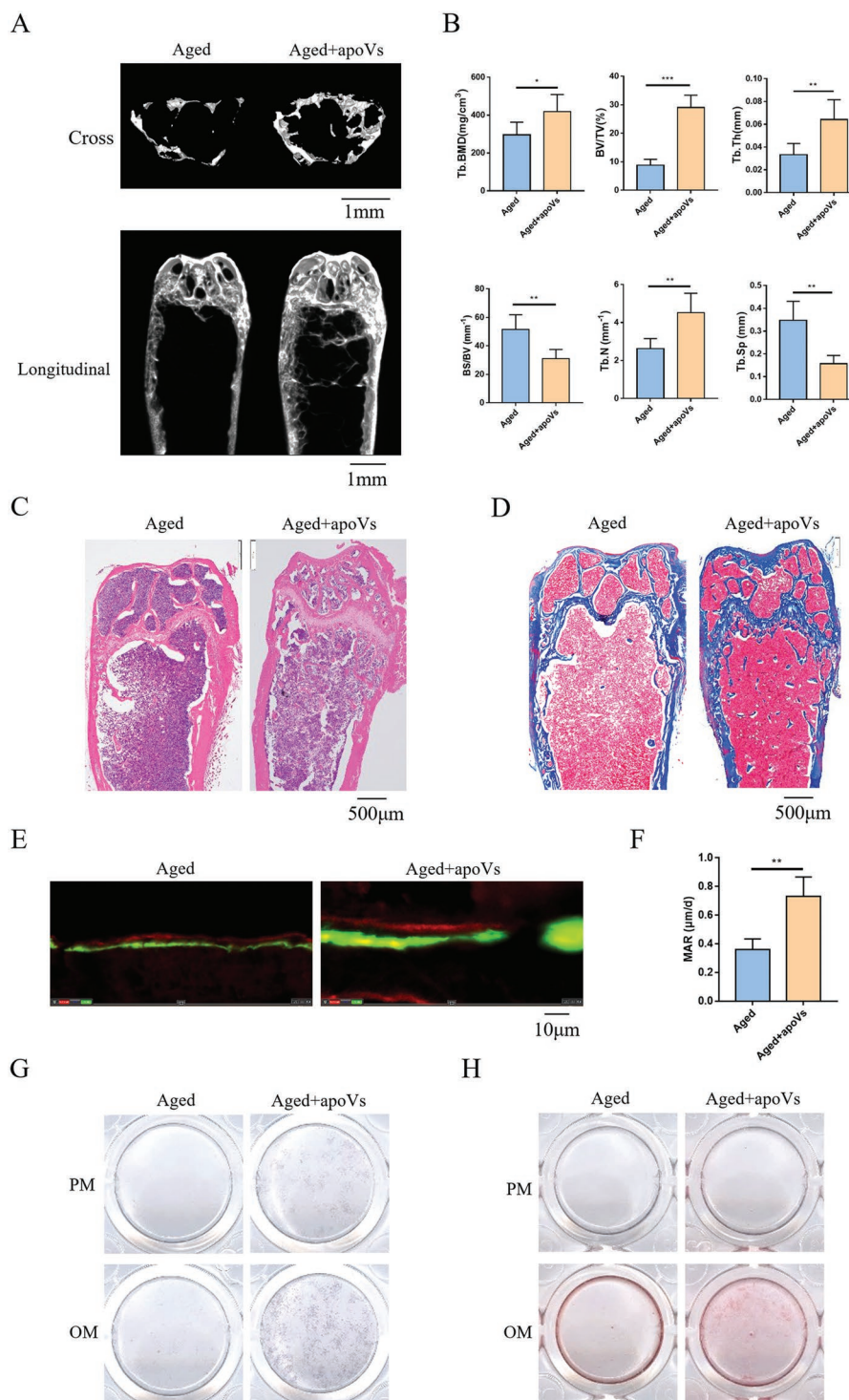


Figure 5. ApoVs prevent a decrease in bone mass and the deterioration of bone microarchitecture in aged mice. A) Representative images of the femur reconstructed by micro-CT. B) Bone histomorphometry of the femur. C) H&E staining. D) Masson staining. E) Representative fluorescence images of the femur obtained after double labeling. F) Dynamic MAR measured from the femur. BMMSCs extracted from mouse femurs from the different groups were stained G) with ALP on day 7 and H) with ARS on day 14. * $P < 0.05$, ** $P < 0.01$, *** $P < 0.001$. $N \geq 5$ per group.

different biological processes,^[75] including the transfer of biomolecules to recipient cells and intercellular communication.^[76] Numerous studies have demonstrated that RNAs encapsulated in EVs can be transported to recipient cells, where they alter the

expression of target genes and therefore cellular function.^[77–80] We performed RT-qPCR to test the expressions of various miRNAs associated with bone metabolism in apoVs. The results showed the different expression profiles of these miRNAs in

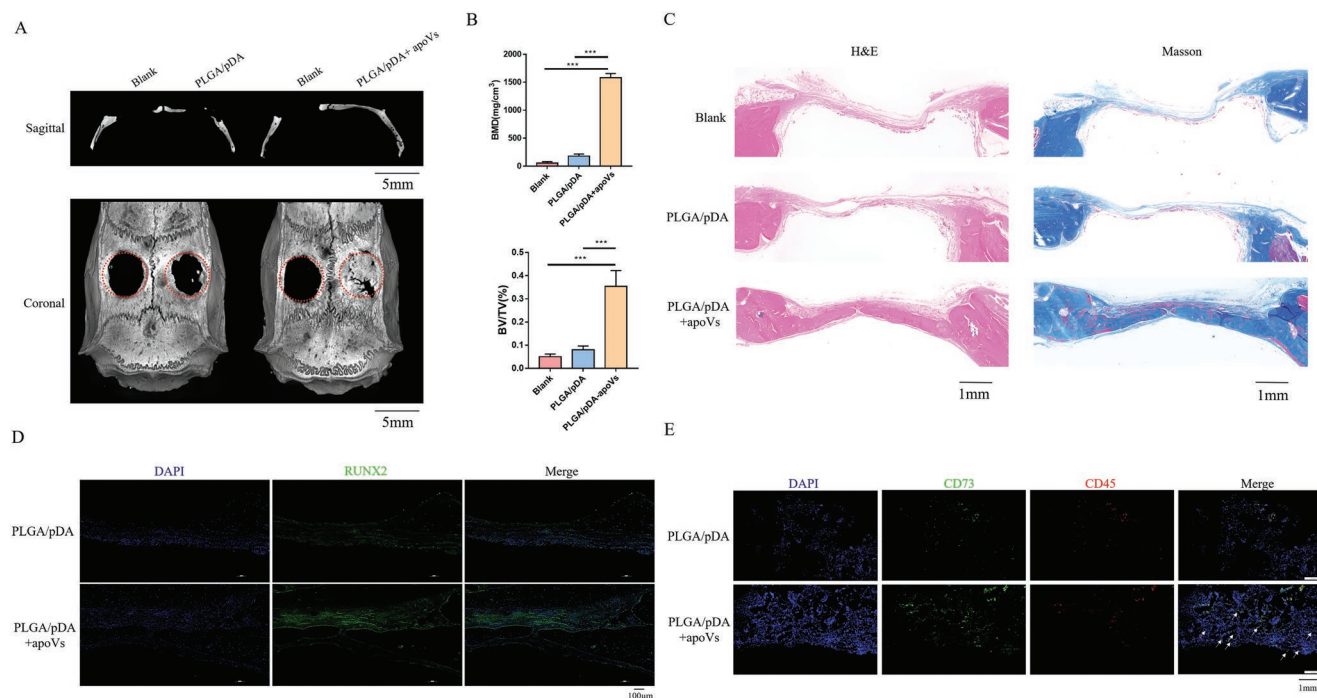


Figure 6. ApoVs increase bone formation in rat calvarial defects. A) Micro-CT images B) Bone histomorphometry of new bone among the groups. C) H&E and Masson staining. D) Immunofluorescence staining of RUNX2. E) Immunofluorescence staining showed significantly more *in vivo* recruitment of CD73+/CD45⁺MSCs (white arrows) by the PLGA/pDA + apoVs group than by the PLGA/pDA group after 1 week of implantation. *** $P < 0.001$. $N \geq 5$ per group.

apoVs, and miR1324 was the highest enriched miRNA in apoVs (Figure 8A). The many properties of miR1324 include the inhibition of cell proliferation, the induction of apoptosis, and the reduction of cell migration and invasion in hepatocellular carcinoma, laryngeal squamous cell carcinoma, papillary thyroid

carcinoma, glioma, and non-small cell lung cancer, by targeting multiple oncogenes.^[81–85] However, there are no studies on the role of miR1324 on stem cell osteogenesis. We, therefore, transfected MSCs with inhibitor-negative control (inhi-NC), inhibitor-miR1324 (inhi-miR1324), mimic-negative control (miR-NC),

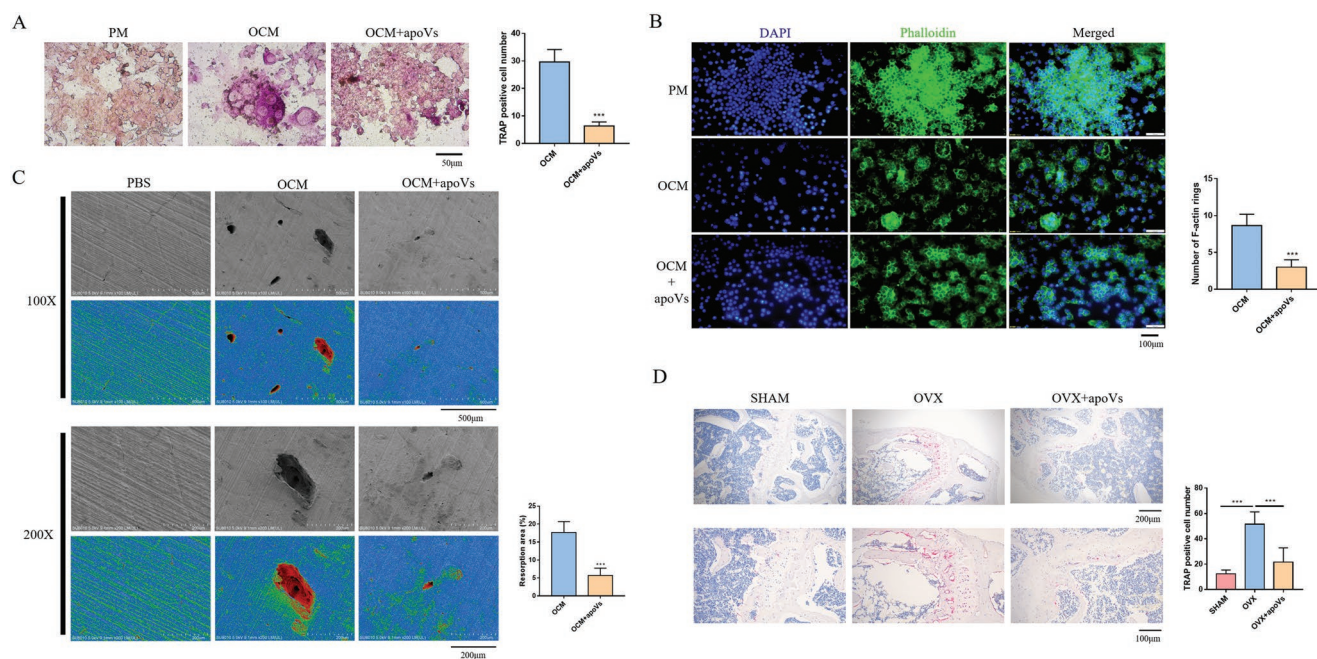


Figure 7. ApoVs inhibits bone resorption. ApoVs inhibit osteoclast formation as indicated by A) TRAP staining and B) fluorescence staining. C) ApoVs inhibit bone resorption as indicated in a bone resorption assay. D) Representative images of TRAP-stained femur slices. *** $P < 0.001$. $N \geq 5$ per group.

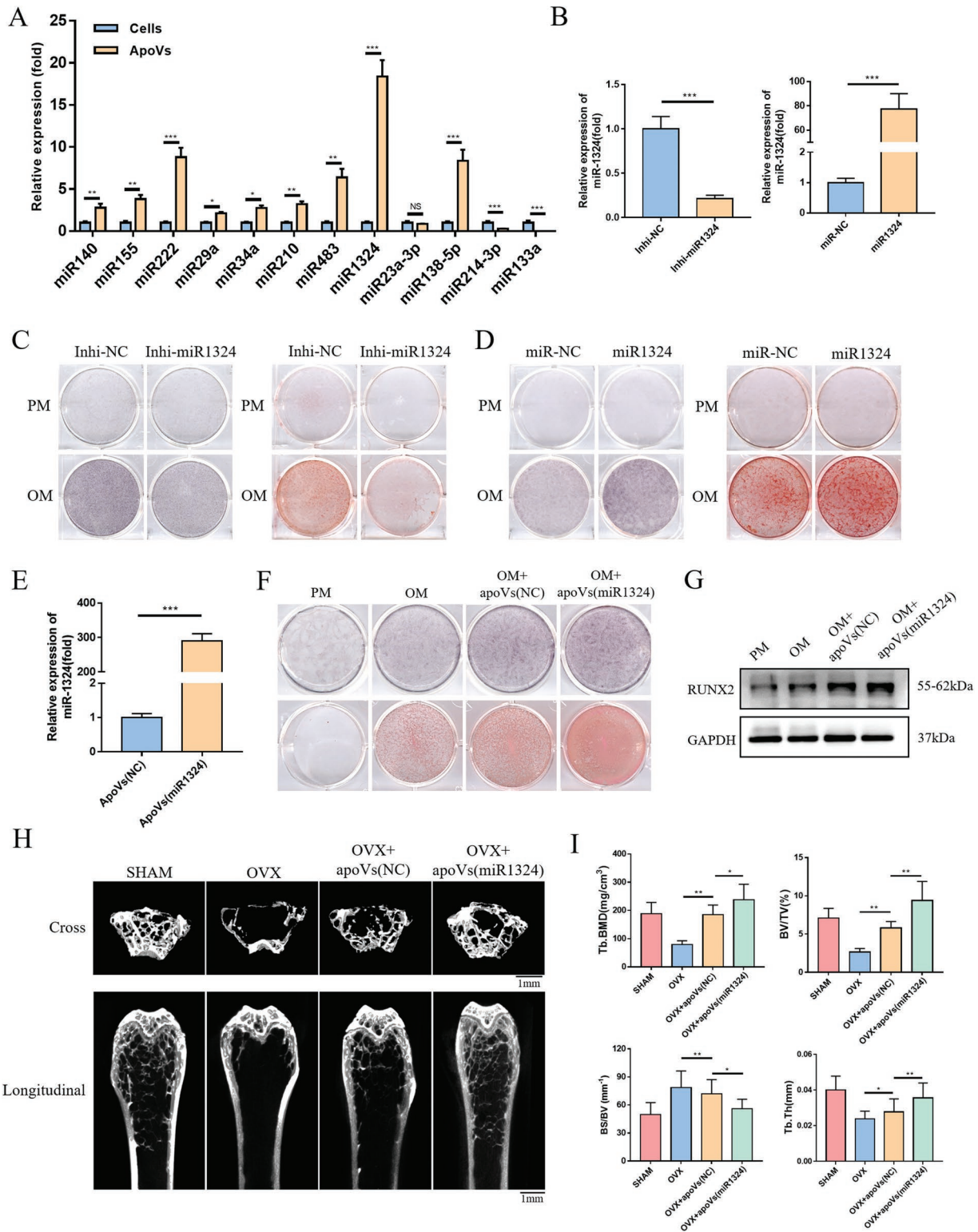


Figure 8. MiR1324 promotes osteogenesis by MSCs. A) Expression levels of different miRNAs in hBMMSCs and apoVs. B) Expression levels of miR1324 in transfected MSCs. ALP and ARS staining of MSCs transfected C) with Inhi-NC and Inhi-miR1324 and D) with miR-NC and miR1324. E) Expression levels of miR1324 in apoVs (NC) and apoVs (miR1324). F) ALP and ARS staining of MSCs cultured with apoVs (NC) and apoVs (miR1324). G) Western blotting. H) Representative images of femur reconstructed by micro-CT. I) Histomorphometry of the femur. NS, not significant, * $P < 0.05$, ** $P < 0.01$, *** $P < 0.001$. $N \geq 5$ per group.

and mimic-miR1324 (Figure 8B). The expression level of miR1324 in MSCs was significantly reduced by inhi-miR1324 and increased by miR1324. Next, osteogenesis was induced in MSCs with knocked-down or overexpressed miR1324. ALP and ARS staining showed that miR1324 knockdown inhibited and miR1324 overexpression promoted osteogenesis (Figure 8C,D). These results indicate that miR1324 promotes osteogenesis in MSCs. Then apoptosis was induced in the miR-NC- and mimic-miR1324-treated groups and their apoVs, i.e., apoVs (NC), and apoVs (miR1324), were extracted. miR1324 expression was significantly higher in apoVs (miR1324) than in apoVs (NC) (Figure 8E). ALP and ARS staining of MSCs treated with apoVs (miR1324) showed that miR1324 promoted osteogenesis (Figure 8F). In Western blotting, RUNX2 expression was higher in MSCs treated with apoVs (miR1324) than with apoVs (NC) (Figure 8G). Next, apoVs (NC) and apoVs (miR1324) were injected into OVX mice via tail veins, and the histomorphology of the femur was assessed via micro-CT (Figure 8H). Tb.BMD, BV/TV, BS/BV, and Tb.Sp were significantly higher in the apoVs (miR1324) group than in the apoVs (NC) group (Figure 8I). These results suggest that miR1324 enhances the therapeutic effect of apoVs on bone loss in OVX mice.

2.9. MiR1324 Inhibits Osteoblast Differentiation of RAW264.7 Cells

The role of miR1324 in osteoclast differentiation, and thus on bone resorption, was analyzed in RAW264.7 cells (Figure 9). TRAP staining showed fewer osteoclasts in the OCM + apoVs (miR1324) group than in the OCM + apoVs (NC) group. In bone resorption assays, the area of bone resorption was smaller in the OCM + apoVs (miR1324) group than in the OCM + apoVs (NC). Fluorescence staining and Western blotting revealed fewer osteoclasts and less TRAP expression, respectively, in the OCM + apoVs (miR1324) group than in the OCM + apoVs (NC) group. The results indicate that the inhibition of bone resorption by apoVs is at least in part mediated by the inhibition of osteoclast formation by miR1324.

2.10. Overexpression of miR1324 Inhibits SNX14 by Targeting its 3'-UTR

MiRNA regulates the expression of target genes mainly by binding to their 3'-UTRs.^[86] To investigate the molecular mechanism by which miR1324 regulates osteogenesis in MSCs, we used TargetScan software to examine important target genes of miR1324, which identified *Sorting Nexin 14* (*SNX14*) (Figure 10). The putative binding site of miR1324 on the 3'-UTR of *SNX14* was determined using miRbase software. Next, a luciferase assay was performed, which showed that miR1324 inhibited luciferase expression by vectors containing the 3'-UTR of wild-type but not mutant *SNX14*, thus demonstrating the binding of miR1324 to the *SNX14* 3'-UTR to inhibit *SNX14* expression. Extracted RNA from the miR1324-overexpressing (miR1324) and control (miR-NC), and performed RT-qPCR, the results showed a decrease in *SNX14* expression. In a subsequent experiment, *SNX14* knockdown was achieved by transfecting MSCs with siSNX14. Both RT-qPCR and Western blotting confirmed

the knockdown of *SNX14* at the RNA and protein levels. Then MSCs with *SNX14* knockdown were used to examine the effect of *SNX14* on osteogenesis in MSCs. ALP and ARS staining showed the osteogenic ability of MSCs was enhanced following *SNX14* knockdown. RT-qPCR showed the increased expression of *RUNX2* after *SNX14* knockdown. An examination of osteogenesis-related signaling pathways by Western blotting and semi-quantitative protein determination showed the activation of the SMAD1/5 pathway of MSCs and the significantly increased expression of P-SMAD1/5 and *RUNX2* after *SNX14* knockdown. These results suggest that miR1324 inhibits *SNX14* expression by binding to its 3'-UTR and further activates the SMAD1/5 pathway, thus promoting osteogenesis in MSCs.

2.11. hBMMS-C-Derived apoVs Promote MSC Osteogenesis and Inhibit Osteoclast Differentiation via the SMAD1/5 Signaling Pathway

In investigating the mechanism by which apoVs regulate MSC osteogenesis, we found that SMAD1/5 phosphorylation was significantly increased in MSCs cultured with apoVs (Figure 11). Thus, next, we used LDN-193189, which inhibits BMP-mediated Smad1 and Smad5 activation,^[87] to examine whether the ability of apoVs to promote MSC osteogenesis involves SMAD1/5 signaling. ALP and ARS staining indicated LDN-193189 could reverse the osteogenesis-promoting effect of apoVs on MSCs. SMAD1/5 phosphorylation was significantly decreased in MSCs cultured with apoVs in OM and treated with LDN-193189. Subsequently, we verified that miR1324 activated the SMAD1/5 pathway, thus promoting the osteogenic differentiation of MSCs. Western blotting of RAW264.7 cells showed that SMAD1/5 activation was inhibited after their osteoblastic induction, whereas apoVs could activate the SMAD1/5 pathway. And apoVs (miR1324) could further activate the SMAD1/5 pathway than apoVs (NC). Taken together, these results indicate that hBMMS-C-derived apoVs positively regulate MSC osteogenesis and negatively regulate osteoclast differentiation by activating the SMAD1/5 signaling pathway.

3. Conclusion

This study explored the role of hBMMS-C-apoVs in the maintenance of bone homeostasis and bone defect repair. An investigation of the molecular mechanisms showed that hBMMS-C-derived apoVs regulate bone metabolism via the miR1324/*SNX14*/SMAD1/5 pathway. Although progress has been made in research into the regulatory strategies of bone metabolism, practical clinical translation of that research has been limited. The knowledge gained from our in-depth study of both the regulatory role of hBMMS-C-apoVs in bone homeostasis and bone defects and the underlying mechanisms will contribute to a better understanding of bone repair and regeneration and to new therapeutic approaches to bone defects and bone loss. Because MSC-derived apoVs are easily obtained and stored, with low risks of immunological rejection and neoplastic transformation, they offer a promising approach to the prevention of bone loss and to cell-free bone tissue engineering.

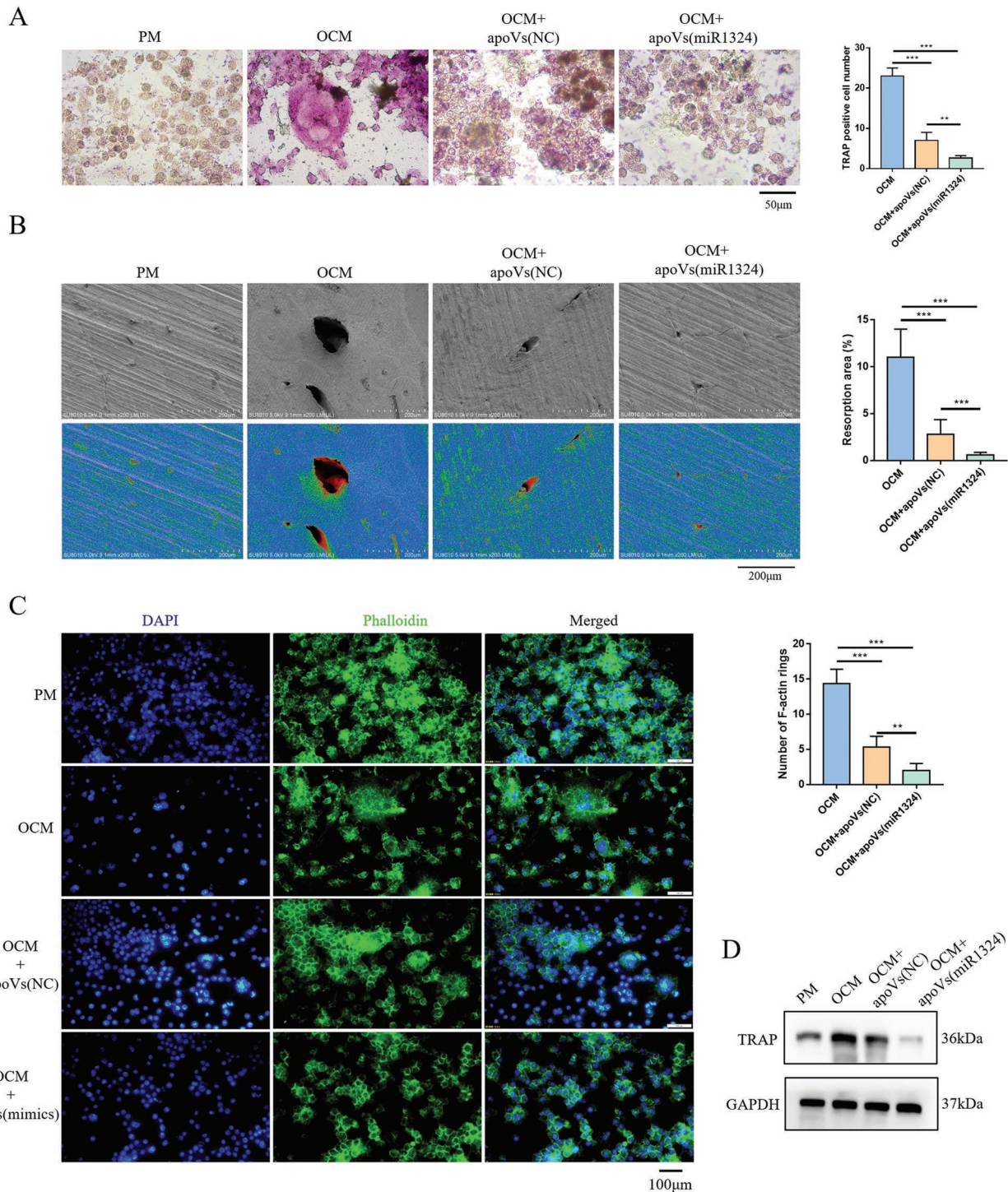


Figure 9. MiR1324 inhibits osteoblast differentiation of RAW264.7 cells as indicated by: A) TRAP staining, B) bone resorption assay, and C) fluorescence staining. D) Western blotting shows less TRAP expression in cells treated with apoVs (miR1324) than in cells treated with apoVs (NC). ** $P < 0.01$, *** $P < 0.001$.

4. Experimental Section

The protocol was approved by the Institutional Animal Care and Use Committee of the Peking University Health Science Center (approval no. LA2022039).

Cell Culture, Osteogenic Induction, and Osteoclastic Induction: hBMMSCs and primary RAW264.7 macrophages cells were obtained

from ScienCell and cultured in α -minimum essential medium (α -MEM) (Gibco, 12 571) or Dulbecco's modified Eagle's medium (DMEM) (Gibco, 11965-092). PM containing 10% (v/v) fetal bovine serum (FBS) (Gibco, 10099–141) and 1% (v/v) antibiotics (Gibco, 15 140 122) in α -MEM or DMEM. OM contained 10% (v/v) FBS, 1% (v/v) antibiotics, 10 nM dexamethasone (Sigma-Aldrich, D1756), 200 μ M ascorbic acid (Sigma-Aldrich, A92902), and 10 mM β -glycerophosphate (Sigma-Aldrich,

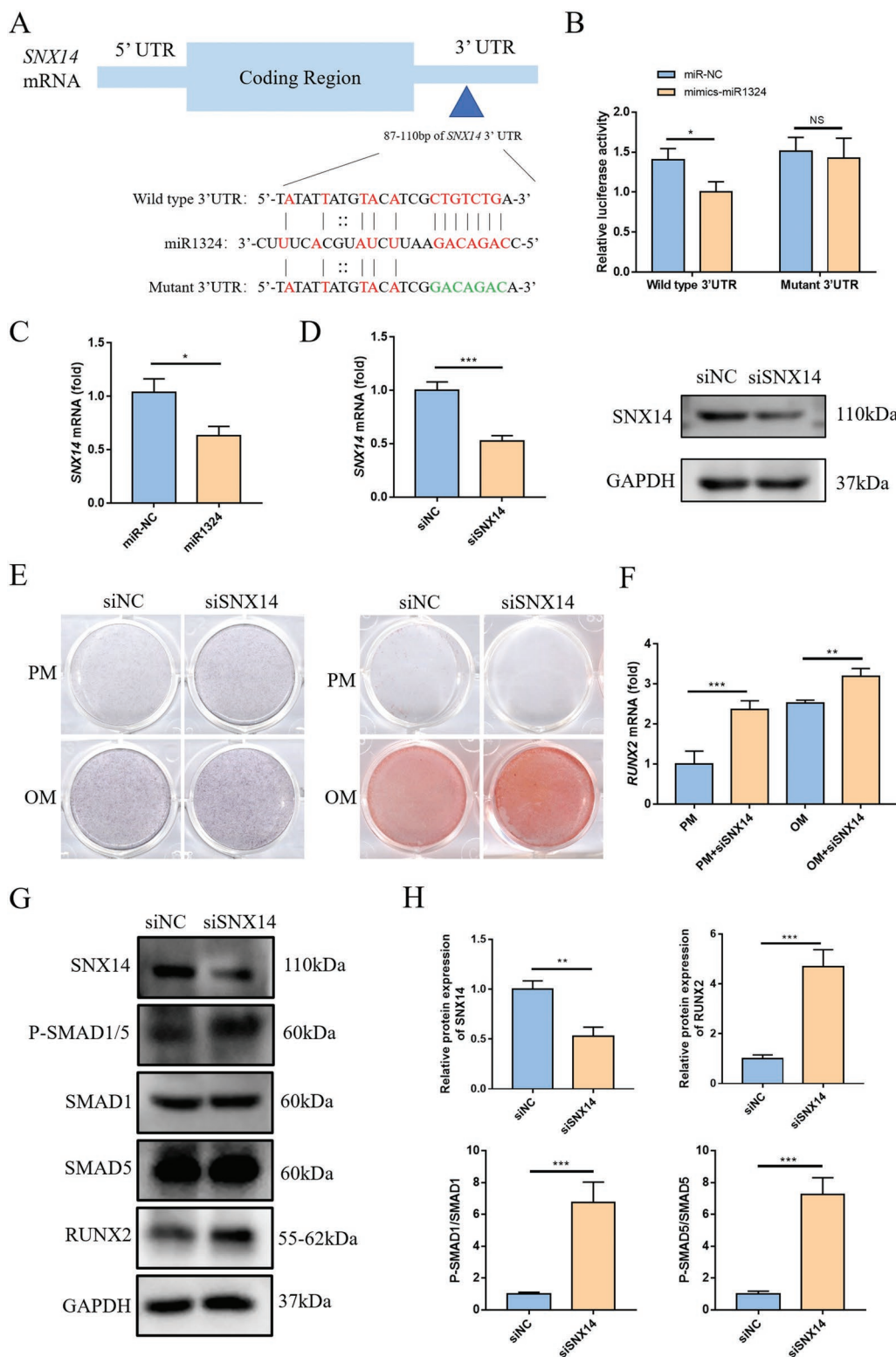


Figure 10. Overexpression of miR1324 inhibits *SNX14* by targeting its 3'-UTR. A) Predicted binding sites of miR1324 in the 3'-UTR of *SNX14*-WT mRNA (mutated bases in the 3'-UTR of *SNX14*-MT mRNA are underlined). B) Luciferase activity of cells overexpressing miR1324 as determined in the *SNX14*-WT and *SNX14*-MT groups. C) Expression levels of *SNX14* in MSCs of the miR-NC and miR1324 groups. D) *SNX14* RNA and protein expression in MSCs of the siNC and siSNX14 groups. E) ALP and ARS staining of MSCs transfected with siNC and siSNX14. F) *RUNX2* expression levels in MSCs transfected with siNC and siSNX14. G) Western blotting of the SMAD1/5 pathway in MSCs after knockdown of *SNX14*. H) Relative protein levels in MSCs after *SNX14* knockdown. NS, not significant, * $P < 0.05$, ** $P < 0.01$, *** $P < 0.001$.

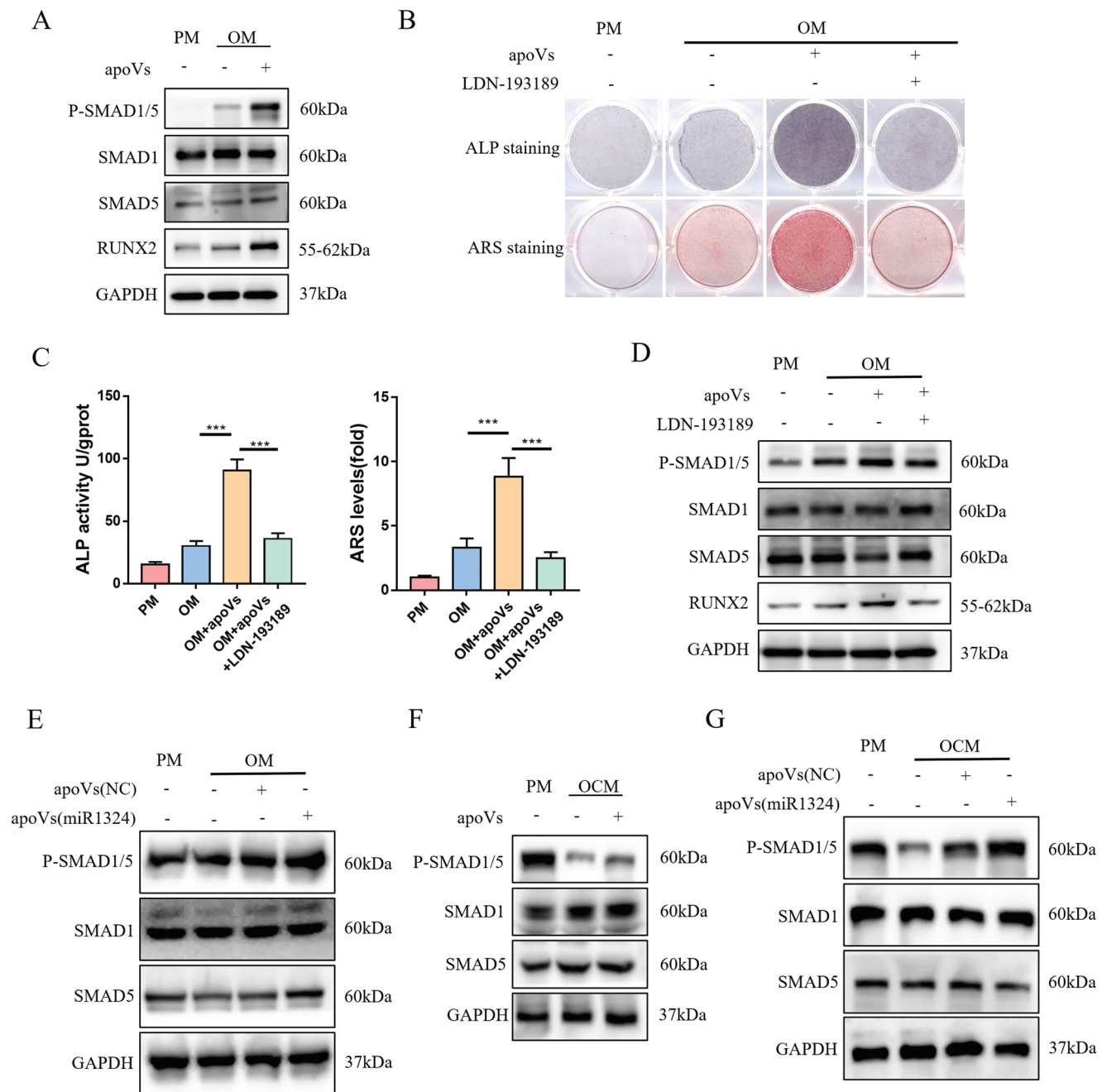


Figure 11. hBMMSC-derived apoVs promote MSC osteogenesis of MSCs and inhibit osteoclast differentiation via the SMAD1/5 signaling pathway. A) ApoVs activate the SMAD1/5 pathway. B) ALP and ARS staining and C) ALP and ARS quantification of MSCs cultured with apoVs and LDN-193189. D) Phosphorylation of SMAD1/5 is significantly decreased in MSCs cultured with apoVs in OM and treated with LDN-193189. E) The SMAD1/5 pathway is activated in cells treated with apoVs (miR1324) compared to the group treated with apoVs (NC). F) ApoVs activate the SMAD1/5 pathway during the osteoclastic differentiation of RAW264.7 cells. G) The SMAD1/5 pathway is activated in cells treated with apoVs (miR1324) compared to cells treated with apoVs (NC). *** $P < 0.001$.

G5422). Osteoclastic medium (OCM) contained 10% (v/v) FBS, 1% (v/v) antibiotics, and 100 ng mL⁻¹ RANKL (R&D Systems, 462-TEC-010).

TUNEL Staining: Cell apoptosis was detected using the TUNEL cell apoptosis detection kit (Appligen, C0003-20) in normal or apoptotic MSCs fixed and then treated with 0.2% Triton X-100 (Sigma-Aldrich, 93 443). Fluorescence microscopy (Olympus) images were obtained from cells exposed to rhodamine fluorescein (red) labeled dUTP solution in the dark for 1 h.

Isolation and Purification of apoVs: ApoVs were collected as previously described, with modifications.^[35,36] The Pierce BCA protein assay kit (Thermo Scientific, 23 227) was used to determine their concentration.

Identification of apoVs: The morphology of the apoVs was observed by TEM. The apoVs were fixed, placed dropwise onto a copper mesh coated with carbon, dried, and then stained twice with 1% uranyl acetate. Images were captured using HT7700 TEM (Hitachi). The particle size of the apoVs was determined using Nano Sight NS300 (Malvern). Surface

markers of MSC-derived apoVs were identified by flow cytometry, as described in the previous study.^[35] Western blotting of apoV surface marker proteins was performed as previously described.^[88]

ApoV Uptake by MSCs: ApoVs labeled with PKH-26 (Sigma-Aldrich, PKH26GL) were washed in filtered PBS at 16 000 g for 30 min, incubated with MSCs, fixed, treated with 0.1% TritonX-100 at room temperature for 7 min, and washed twice with PBS. Then 5 $\mu\text{g mL}^{-1}$ FITC-Cyclopeptide (Sigma-Aldrich, P5282) was added. Cell nuclei were stained with 6-diamidino-2-phenylindole (DAPI, Sigma-Aldrich, MBD0015). Images were taken using the LSM 5 EXCITER (Carl Zeiss).

ALP Staining and Activity, ARS Staining and Quantification, and TRAP Staining: ALP staining of MSCs was stained using the NBT/BCIP staining kit (CoWin Biotech, C3206). ALP activity was quantified using the ALP assay kit (Nanjing Jiancheng Bioengineering Institute, A059-2-2). The absorbance measured at 520 nm was used to calculate ALP activity. On day 14 after osteogenic induction, the MSCs were stained with 2% ARS (Sigma-Aldrich, A5533). Mineral accumulation was quantified by adding 100 mM cetylpyridine and then measuring the absorbance at 562 nm after the cells had completely dissolved.

RAW264.7 cells were divided into PM and OCM groups and on day 4 after osteoclastic induction were stained for TRAP using the TRAP staining kit (Sigma-Aldrich, CS0740).

Real-Time Quantitative PCR: Total cellular RNA was extracted using TRIzol reagent (Invitrogen, 15 596 026). cDNA was synthesized using the PrimeScript RT reagent kit (Takara, RR037A) and RT-qPCR was conducted using SYBR Green Master Mix on an ABI Prism 7500 real-time PCR System. The miDETECT A Track miRNA qRT-PCR Starter Kit (Ribobio, C10712-1) was used to detect miRNA expression, and the miDETECT A Track miRNA qRT-PCR Primer (Ribobio, miracm001-12) was used as primers for different miRNAs. *GAPDH* and *U6* served as the reference genes. The primer sequences are listed in Table 1.

Western Blotting Analysis: Protein extracts prepared by lysing the cells with RIPA containing 2% proteinase inhibitor were subjected to SDS-PAGE on a 10% polyacrylamide gel and transferred to a PVDF membrane. The membrane was incubated with the primary and secondary antibodies. The protein bands were detected using an enhanced chemiluminescence kit (Applygen, PI050). The reagent numbers of the antibodies were listed in Table 2.

In vivo Implantation of MSCs and the Evaluation of Ectopic Bone Tissue Formation: MSCs cultured with or without apoVs (group control and apoVs) were mixed with β -tricalcium phosphate (TCP; RB-SK-005 G). Six-week-old female BALB/C nude mice were anesthetized, the surgical site was sterilized, the subcutaneous implantation cavity was separated and the cell-scaffold mixtures were implanted and sutured in position. The operation was carried out in a specific-pathogen-free (SPF) animal surgery room. Mouse tissues were harvested after 8 weeks and examined via H&E and Masson's trichrome staining.

Tail Vein Injection in OVX and Aged Mice: A mouse model mimicking estrogen-deficiency-induced bone loss was created by subjecting 8-week-old mice to bilateral oophorectomy. A sham-operated group was established as well. First, different concentration gradients were set, and the optimal concentration of apoVs was screened. The OVX mice were randomly grouped into OVX and OVX + apoVs groups. ApoVs were injected weekly (8 weeks after bilateral oophorectomy) via the tail vein. Aged mice consisted of 18-month-old female mice, which after 1-week acclimatization were randomly assigned to the aged or aged + apoVs group, in which apoVs were injected via the tail vein. Two months after apoV injection, all mice were anesthetized and then euthanized. The femurs were fixed in 4% paraformaldehyde for 1 week. Tissues scanned by micro-CT were decalcified in 10% EDTA (pH 7.4), and stained with H&E or Masson.

Dynamic Histomorphometric Analyses: The mice were intraperitoneally injected with calcein and alizarin-3-methyliminodiacetic acid 10 days and 3 days before they were euthanized. The femur of the euthanized mice was removed and fixed. The MAR was determined using Bioquant software.

Construction of Novel Cell-Free Tissue-Engineered Bone from apoVs and a PLGA/pDA Scaffold: As in a previous study,^[44] the scaffolds were immersed in 1 $\mu\text{g apoVs } \mu\text{L}^{-1}$ for 12 h at 4 °C. Then scaffolds incubated with apoVs were incubated in saline at 37 °C and the supernatants were

collected over 1–6 days to measure apoV release. The surface morphology of the different scaffold preparations was observed by SEM.

Cranial Defects in Rats: Five-week-old male SD rats were divided into three groups: blank; PLGA/pDA scaffold (PLGA/pDA group); and PLGA/pDA scaffold + apoVs (PLGA/pDA + apoVs group). The rat calvaria were subjected to two 5 mm diameter defects created with a low-speed trephine burr. Following the implantation of the scaffolds into the defects, the incision was stitched. After the removal of the scaffolds, they were scanned by micro-CT, decalcified in 10% EDTA (pH 7.4), and stained with H&E or Masson.

Micro-CT Analyses: Samples were scanned using the Inveon MM System (Siemens) micro-CT. Software from Siemens' Inveon Research Workplace was used to do the parametric analysis. An area of the femur located 0.5–1 mm proximal to the epiphysis was analyzed with respect to BV/TV, Tb.Th, Tb.N, and Tb.Sp. New bone volume in the calvarial defects was quantified based on the number of pixels in the region of interest.

Dual Luciferase Analysis Experiment: The hBMMSCs were cultured in a 24-well plate and cotransfected with 100 nM negative control or miR1324 mimics, 1 $\mu\text{g SNX14-WT}$ or SNX14-MT luciferase reporter plasmid and lipofectamine 3000 (Invitrogen, L3000-008). After 48 h, the dual-luciferase reporter assay system (Promega, E1910) was used to detect luciferase activities.

siRNA Transient Infection: siRNAs were purchased from Sangon Biotech. The sequences were listed in Table 1. When MSCs reached 60–70% density, siRNAs were transfected into MSCs using lipofectamine 3000 (Invitrogen, L3000-008).

Statistical Analysis: SPSS 19.0 software was used for the statistical analysis. The results are expressed as the mean \pm standard deviation. Differences between two groups were analyzed in an independent two-tailed Student's *t*-test. One-way ANOVA and a Tukey's post hoc test were used for comparisons between groups. *P*-values <0.05 were considered to indicate statistical significance.

Supporting Information

Supporting Information is available from the Wiley Online Library or from the author.

Acknowledgements

This study was supported by grants from the Beijing Natural Science Foundation (No. 7222224 to XZ, No. L222090 to YL), the National Natural Science Foundation of China (No. 82170929 and 81970908 to YL).

Conflict of Interest

The authors declare no conflict of interest.

Data Availability Statement

The data that support the findings of this study are available from the corresponding author upon reasonable request.

Keywords

apoptotic vesicles, bone metabolism, cell-free therapy, miR1324/SNX14/SMAD1/5 signaling axis

Received: September 21, 2022
Revised: November 17, 2022
Published online: January 20, 2023

- [1] M. Zaidi, T. Yuen, L. Sun, C. J. Rosen, *Endocr. Rev.* **2018**, *39*, 701.
- [2] T. Nakashima, M. Hayashi, T. Fukunaga, K. Kurata, M. Oh-Hora, J. Q. Feng, L. F. Bonewald, T. Kodama, A. Wutz, E. F. Wagner, J. M. Penninger, H. Takayanagi, *Nat. Med.* **2011**, *17*, 1231.
- [3] S. L. Teitelbaum, *Science* **2000**, *289*, 1504.
- [4] K. Nakahama, *Cell. Mol. Life Sci.* **2010**, *67*, 4001.
- [5] A. Cappariello, A. Maurizi, V. Veeriah, A. Teti, *Arch. Biochem. Biophys.* **2014**, *558*, 70.
- [6] A. Ho-Shui-Ling, J. Bolander, L. E. Rustom, A. W. Johnson, F. P. Luyten, C. Picart, *Biomaterials* **2018**, *180*, 143.
- [7] R. W. Keen, *Curr. Osteoporos. Rep.* **2003**, *1*, 66.
- [8] L. A. Armas, R. R. Recker, *Endocrinol. Metab. Clin. North Am.* **2012**, *41*, 475.
- [9] P. Yang, J. Zhou, Q. Ai, B. Yu, M. Deng, F. Luo, Z. Xie, J. Xing, T. Hou, *Cell Transplant.* **2020**, *29*, 963689720940722.
- [10] A. Uccelli, L. Moresca, V. Pistoia, *Nat. Rev. Immunol.* **2008**, *8*, 726.
- [11] A. J. Leo, D. A. Grande, *Cells Tissues Organs* **2006**, *183*, 112.
- [12] J. Galipeau, L. Sensébé, *Cell Stem Cell* **2018**, *22*, 824.
- [13] S. Wang, X. Qu, R. C. Zhao, *Front. Med.* **2011**, *5*, 372.
- [14] Y. Zhu, P. Zhang, R. L. Gu, Y. S. Liu, Y. S. Zhou, *Chin. J. Dent. Res.* **2018**, *21*, 89.
- [15] K. Sellheyer, D. Krahl, *J. Am. Acad. Dermatol.* **2010**, *63*, 859.
- [16] J. Bartunek, A. Behfar, D. Dolatabadi, M. Vanderheyden, M. Ostojic, J. Dens, B. El Nakadi, M. Banovic, B. Beleslin, M. Vrolix, V. Legrand, C. Vrints, J. L. Vanoverschelde, R. Crespo-Diaz, C. Homys, M. Tendera, S. Waldman, W. Wijns, A. Terzic, *J. Am. Coll. Cardiol.* **2013**, *61*, 2329.
- [17] J. He, N. Zhang, Y. Zhu, R. Jin, F. Wu, *Biomaterials* **2021**, *265*, 120448.
- [18] X. Wang, H. Chen, X. Zeng, W. Guo, Y. Jin, S. Wang, R. Tian, Y. Han, L. Guo, J. Han, Y. Wu, L. Mei, *Acta Pharm. Sin. B* **2019**, *9*, 167.
- [19] Y. Zhu, X. Zhang, R. Gu, X. Liu, S. Wang, D. Xia, Z. Li, X. Lian, P. Zhang, Y. Liu, Y. Zhou, *Stem Cell Res. Ther.* **2020**, *11*, 135.
- [20] S. Zeitouni, U. Krause, B. H. Clough, H. Halderman, A. Falster, D. T. Blalock, C. D. Chaput, H. W. Sampson, C. A. Gregory, *Sci. Transl. Med.* **2012**, *4*, 132ra55.
- [21] S. Zhang, D. Xie, Q. Zhang, *Pharmacol. Res.* **2021**, *172*, 105851.
- [22] J. S. Hyun, M. C. Tran, V. W. Wong, M. T. Chung, D. D. Lo, D. T. Montoro, D. C. Wan, M. T. Longaker, *Biotechnol. Adv.* **2013**, *31*, 736.
- [23] M. Shafiq, Y. Jung, S. H. Kim, *Biomaterials* **2016**, *90*, 85.
- [24] M. A. Lafamme, K. Y. Chen, A. V. Naumova, V. Muskheli, J. A. Fugate, S. K. Dupras, H. Reinecke, C. Xu, M. Hassanipour, S. Police, C. O'Sullivan, L. Collins, Y. Chen, E. Minami, E. A. Gill, S. Ueno, C. Yuan, J. Gold, C. E. Murry, *Nat. Biotechnol.* **2007**, *25*, 1015.
- [25] K. C. Rustad, V. W. Wong, M. Sorkin, J. P. Glotzbach, M. R. Major, J. Rajadas, M. T. Longaker, G. C. Gurtner, *Biomaterials* **2012**, *33*, 80.
- [26] M. Zhang, D. Methot, V. Poppa, Y. Fujio, K. Walsh, C. E. Murry, *J. Mol. Cell. Cardiol.* **2001**, *33*, 907.
- [27] H. Liu, S. Liu, X. Qiu, X. Yang, L. Bao, F. Pu, X. Liu, C. Li, K. Xuan, J. Zhou, Z. Deng, S. Liu, Y. Jin, *Autophagy* **2020**, *16*, 2140.
- [28] E. T. Roche, C. L. Hastings, S. A. Lewin, D. Shvartsman, Y. Brudno, N. V. Vasylev, F. J. O'Brien, C. J. Walsh, G. P. Duffy, D. J. Mooney, *Biomaterials* **2014**, *35*, 6850.
- [29] A. M. Parr, I. Kulbatski, C. H. Tator, *J. Neurotrauma* **2007**, *24*, 835.
- [30] S. Liu, L. Jiang, H. Li, H. Shi, H. Luo, Y. Zhang, C. Yu, Y. Jin, *J. Invest. Dermatol. Symp. Proc.* **2014**, *134*, 2648.
- [31] R. Singh, A. Letai, K. Sarosiek, *Nat. Rev. Mol. Cell Biol.* **2019**, *20*, 175.
- [32] S. Arandjelovic, K. S. Ravichandran, *Nat. Immunol.* **2015**, *16*, 907.
- [33] B. Fadeel, S. Orrenius, *J. Intern. Med.* **2005**, *258*, 479.
- [34] S. Caruso, I. K. H. Poon, *Front. Immunol.* **2018**, *9*, 1486.
- [35] X. Zhang, J. Tang, X. Kou, W. Huang, Y. Zhu, Y. Jiang, K. Yang, C. Li, M. Hao, Y. Qu, L. Ma, C. Chen, S. Shi, Y. Zhou, *J. Extracell. Vesicles* **2022**, *11*, 11:e12240.
- [36] C. Zheng, B. Sui, X. Zhang, J. Hu, J. Chen, J. Liu, D. Wu, Q. Ye, L. Xiang, X. Qiu, S. Liu, Z. Deng, J. Zhou, S. Liu, S. Shi, Y. Jin, *J. Extracell. Vesicles* **2021**, *10*, 12109.
- [37] J. Wang, Z. Cao, P. Wang, X. Zhang, J. Tang, Y. He, Z. Huang, X. Mao, S. Shi, X. Kou, *ACS Nano* **2021**, *15*, 14360.
- [38] Y. Qu, Y. He, B. Meng, X. Zhang, J. Ding, X. Kou, W. Teng, S. Shi, *Acta Biomater.* **2022**, *149*, 258.
- [39] L. Ma, C. Chen, D. Liu, Z. Huang, J. Li, H. Liu, R. T. Kin Kwok, B. Tang, B. Sui, X. Zhang, J. Tang, X. Mao, W. Huang, S. Shi, X. Kou, *Bioact. Mater.* **2023**, *19*, 626.
- [40] R. Wang, M. Hao, X. Kou, B. Sui, M. L. Sanmillan, X. Zhang, D. Liu, J. Tian, W. Yu, C. Chen, R. Yang, L. Sun, Y. Liu, C. Giraudo, D. A. Rao, N. Shen, S. Shi, *Bioact. Mater.* **2022**, <https://doi.org/10.1016/j.bioactmat.2022.07.026>.
- [41] D. Liu, X. Kou, C. Chen, S. Liu, Y. Liu, W. Yu, T. Yu, R. Yang, R. Wang, Y. Zhou, S. Shi, *Cell Res.* **2018**, *28*, 918.
- [42] R. Mirzayans, D. Murray, *Int. J. Mol. Sci.* **2020**, *21*.
- [43] S. Chen, Y. Tang, Y. Liu, P. Zhang, L. Lv, X. Zhang, L. Jia, Y. Zhou, *Cell Proliferation* **2019**, *52*, 12669.
- [44] W. Li, Y. Liu, P. Zhang, Y. Tang, M. Zhou, W. Jiang, X. Zhang, G. Wu, Y. Zhou, *ACS Appl. Mater. Interfaces* **2018**, *10*, 5240.
- [45] R. Marom, I. Shur, R. Solomon, D. Benayahu, *J. Cell. Physiol.* **2005**, *202*, 41.
- [46] T. Wang, S. Guo, H. Zhang, *Biomed Res. Int.* **2018**, *2018*, 3516463.
- [47] N. S. Hwang, C. Zhang, Y. S. Hwang, S. Varghese, *Wiley Interdiscip. Rev.: Syst. Biol. Med.* **2009**, *1*, 97.
- [48] M. Majidinia, A. Sadeghpour, B. Yousefi, *J. Cell. Physiol.* **2018**, *233*, 2937.
- [49] W. Mende, R. Götzl, Y. Kubo, T. Pufe, T. Ruhl, J. P. Beier, *Cells* **2021**, *10*, 975.
- [50] E. Birmingham, G. L. Niebur, P. E. McHugh, G. Shaw, F. P. Barry, L. M. McNamara, *Eur. Cells Mater.* **2012**, *23*, 13.
- [51] H. Tao, W. Li, W. Zhang, C. Yang, C. Zhang, X. Liang, J. Yin, J. Bai, G. Ge, H. Zhang, X. Yang, H. Li, Y. Xu, Y. Hao, Y. Liu, D. Geng, *Pharmacol. Res.* **2021**, *174*, 105967.
- [52] C. Lin, S. Yu, R. Jin, Y. Xiao, M. Pan, F. Pei, X. Zhu, H. Huang, Z. Zhang, S. Chen, H. Liu, Z. Chen, *Theranostics* **2019**, *9*, 3780.
- [53] W. L. You, Z. L. Xu, *J. Orthop. Surg. Res.* **2021**, *16*, 279.
- [54] M. Qi, L. Zhang, Y. Ma, Y. Shuai, L. Li, K. Luo, W. Liu, Y. Jin, *Theranostics* **2017**, *7*, 884.
- [55] M. Kang, V. Jordan, C. Blenkinsop, L. W. Chamley, *J. Extracell. Vesicles* **2021**, *10*, 12085.
- [56] P. Zhang, B. Dong, E. Zeng, F. Wang, Y. Jiang, D. Li, D. Liu, *Anal. Chem.* **2018**, *90*, 11198.
- [57] S. W. Wen, J. Sceneay, L. G. Lima, C. S. Wong, M. Becker, S. Krumeich, R. J. Lobb, V. Castillo, K. N. Wong, S. Ellis, B. S. Parker, A. Möller, *Cancer Res.* **2016**, *76*, 6816.
- [58] G. Turgeman, Y. Zilberman, S. Zhou, P. Kelly, I. K. Moutsatsos, Y. P. Kharode, L. E. Borella, F. J. Bex, B. S. Komm, P. V. Bodine, D. Gazit, *J. Cell. Biochem.* **2002**, *86*, 461.
- [59] Y. Wang, P. Deng, Y. Liu, Y. Wu, Y. Chen, Y. Guo, S. Zhang, X. Zheng, L. Zhou, W. Liu, Q. Li, W. Lin, X. Qi, G. Ou, C. Wang, Q. Yuan, *Nat. Commun.* **2020**, *11*, 5596.
- [60] J. N. Farr, S. Khosla, *Bone* **2019**, *121*, 121.
- [61] W. Chang, R. Kim, S. I. Park, Y. J. Jung, O. Ham, J. Lee, J. H. Kim, S. Oh, M. Y. Lee, J. Kim, M. S. Park, Y. A. Chung, K. C. Hwang, L. S. Maeng, *Mol. Cells* **2015**, *38*, 643.
- [62] E. L. Fong, C. K. Chan, S. B. Goodman, *Biomaterials* **2011**, *32*, 395.
- [63] H. Yu, J. Cheng, W. Shi, B. Ren, F. Zhao, Y. Shi, P. Yang, X. Duan, J. Zhang, X. Fu, X. Hu, Y. Ao, *Acta Biomater.* **2020**, *106*, 328.
- [64] J. A. Siddiqui, N. C. Partridge, *Physiology (Bethesda, Md.)* **2016**, *31*, 233.
- [65] Q. Chen, P. Shou, C. Zheng, M. Jiang, G. Cao, Q. Yang, J. Cao, N. Xie, T. Velletri, X. Zhang, C. Xu, L. Zhang, H. Yang, J. Hou, Y. Wang, Y. Shi, *Cell Death Differ.* **2016**, *23*, 1128.
- [66] J. Li, X. Chen, L. Lu, X. Yu, *Cytokine Growth Factor Rev.* **2020**, *52*, 88.

- [67] M. Zaidi, *Nat. Med.* **2007**, *13*, 791.
- [68] E. Terpos, M. Politou, A. Rahemtulla, *Blood Rev.* **2005**, *19*, 125.
- [69] L. Deng, Y. Wang, Y. Peng, Y. Wu, Y. Ding, Y. Jiang, Z. Shen, Q. Fu, *Bone* **2015**, *79*, 37.
- [70] Y. Xie, Y. Chen, L. Zhang, W. Ge, P. Tang, *J. Cell. Mol. Med.* **2017**, *21*, 1033.
- [71] L. Rochette, A. Meloux, E. Rigal, M. Zeller, Y. Cottin, C. Vergely, *Int. J. Mol. Sci.* **2019**, *20*, 705.
- [72] N. Huynh, L. VonMoss, D. Smith, I. Rahman, M. F. Felemban, J. Zuo, W. J. Rody Jr., K. P. McHugh, L. S. Holliday, *J. Dent. Res.* **2016**, *95*, 673.
- [73] K. O'Brien, K. Breyne, S. Ughetto, L. C. Laurent, X. O. Breakefield, *Nat. Rev. Mol. Cell Biol.* **2020**, *21*, 585.
- [74] G. Qiu, G. Zheng, M. Ge, J. Wang, R. Huang, Q. Shu, J. Xu, *Stem Cell Res. Ther.* **2019**, *10*, 359.
- [75] H. Taipaleenmäki, *Curr. Osteoporos. Rep.* **2018**, *16*, 1.
- [76] M. Groot, H. Lee, *Cells* **2020**, *9*, 1044.
- [77] B. Dhondt, Q. Rousseau, O. De Wever, A. Hendrix, *Cell Tissue Res.* **2016**, *365*, 621.
- [78] R. Garcia-Martin, G. Wang, B. B. Brandão, T. M. Zanotto, S. Shah, S. Kumar Patel, B. Schilling, C. R. Kahn, *Nature* **2022**, *601*, 446.
- [79] M. A. Mori, R. G. Ludwig, R. Garcia-Martin, B. B. Brandão, C. R. Kahn, *Cell Metab.* **2019**, *30*, 656.
- [80] M. Schulz-Siegmund, A. Aigner, *Adv. Drug Delivery. Rev.* **2021**, *173*, 89.
- [81] Q. Zhu, G. Lu, Z. Luo, F. Gui, J. Wu, D. Zhang, Y. Ni, *Biochem. Biophys. Res. Commun.* **2018**, *497*, 626.
- [82] H. Weng, L. Zeng, L. Cao, T. Chen, Y. Li, Y. Xu, Y. Peng, Y. Ye, *Mol. Ther.—Nucleic Acids* **2021**, *23*, 811.
- [83] Y. L. Chu, *Riv. Eur. Sci. Med. Farmacol.* **2020**, *24*, 4320.
- [84] X. Y. Zhang, Y. Y. Xu, W. Y. Chen, *Riv. Eur. Sci. Med. Farmacol.* **2020**, *24*, 4766.
- [85] L. Liu, T. Dong, J. Sheng, *Cancer Manage. Res.* **2021**, *13*, 6031.
- [86] D. P. Bartel, *Cell* **2009**, *136*, 215.
- [87] Z. Li, S. Xiang, Z. Lin, E. N. Li, H. Yagi, G. Cao, L. Yocum, L. Li, T. Hao, K. K. Bruce, M. R. Fritch, H. Hu, B. Wang, P. G. Alexander, K. A. Khor, R. S. Tuan, H. Lin, *Biomaterials* **2021**, *277*, 121082.
- [88] Y. Zhu, X. Zhang, K. Yang, Y. Shao, R. Gu, X. Liu, H. Liu, Y. Liu, Y. Zhou, *Stem Cell Res. Ther.* **2022**, *13*, 323.